Supporting Information

Enhancing the potential of $Cs_{0.1}MA_{0.9}PbI_3$ perovskite layer through the suspension of pure and vanadium-doped metal sulphides for solar cells

Dhanasekaran Vikraman[a], Hailiang Liu[b], Sajjad Hussain[c,d], K. Karuppasamy[e,f], Jungwon Kang[b], Jongwan Jung[c,d], Akram Alfantazi[e,f], Hyun-Seok Kim[a*]

[a] Division of Electronics and Electrical Engineering, Dongguk University-Seoul, Seoul 04620, Republic of Korea.

[b] Convergence Semiconductor Research Center, Department of Electronics and Electrical Engineering, Dankook University, Yongin 16890, Republic of Korea.

[c] Hybrid Materials Center (HMC), Sejong University, Seoul 05006, Republic of Korea.

[d] Department of Nanotechnology and Advanced Materials Engineering, Sejong University, Seoul 05006, Republic of Korea.

[e] Emirates Nuclear Technology Center (ENTC), Khalifa University of Science and Technology, Abu Dhabi 127788, UAE

[f] Department of Chemical and Petroleum Engineering, Khalifa University of Science and Technology, Abu Dhabi 127788, UAE

* Corresponding author's email: hyunseokk@dongguk.edu

S1. Characterization

The electronic configuration of nanostructures was characterized by Raman spectroscope (Renishaw inVia RE04). Energy dispersive analysis combined JEOL JSM-6700F field emission scanning electron microscopy was used to analyze the morphological and compositional properties of synthesized hybrid nanostructures. X-ray photoelectron spectroscopy analysis was performed using PHI 5000 Versa Probe equipped with a monochromatic Al Kα radiation source (25W, 6.7×10^{-8} Pa). The surface topography of prepared active layers was measured using atomic force microscopy (Park Systems XE-150) operating in non-contact mode with 3 μm × 3 μm scan size. UV-vis optical spectroscopy (Optizen 2120UV) was used to measure the absorption spectra of active layer. The current density-voltage (J-V) characteristics were measured in an electrometer (Keithley 6571B) with a solar simulator (San Ei Elec. XES 40S2-CE) using an AM 1.5G-filtered Xe lamp exposure with an intensity of 100 mW/cm^2. Electrochemical impedance spectroscopy measurements were carried out using a PMC-1000 PARSTAT potentiostat under dark conditions at room temperature by applying 0 V bias voltage over a frequency range from 1 MHz to 1 Hz.

The stability of the perovskite solar cells was evaluated under ambient conditions at room temperature. The devices were unencapsulated and exposed to air with a relative humidity of approximately 35%. The stability measurements were carried out under continuous illumination (100 mW·cm^{-2}). The photovoltaic parameters were periodically measured over a total duration of 1000 hours, and the normalized PCE was tracked to assess device degradation. In addition, thermal stability tests were performed by storing the unencapsulated devices at 70 °C in ambient air. The device performance was monitored at regular intervals to evaluate thermal-induced degradation. Multiple devices were measured to ensure reproducibility of the observed trends.

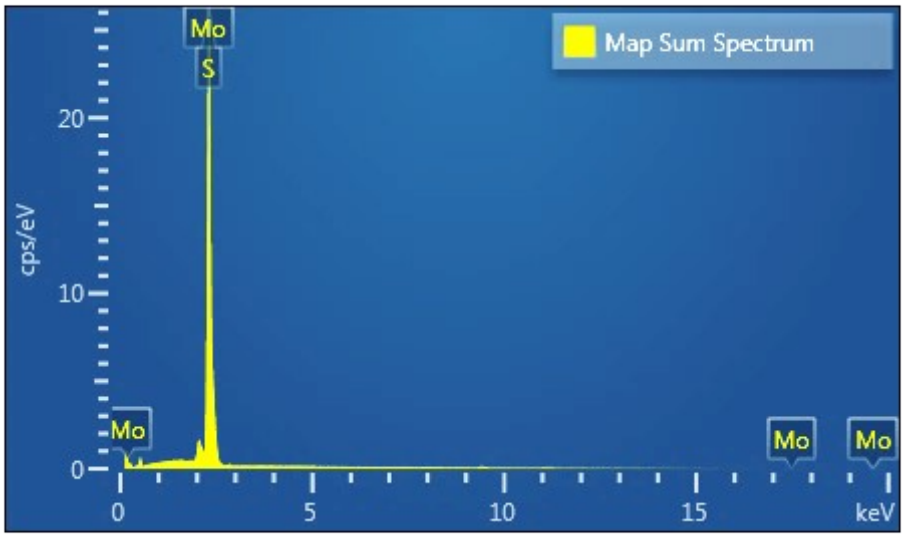

Figure S1. EDS profile of MoS_2.

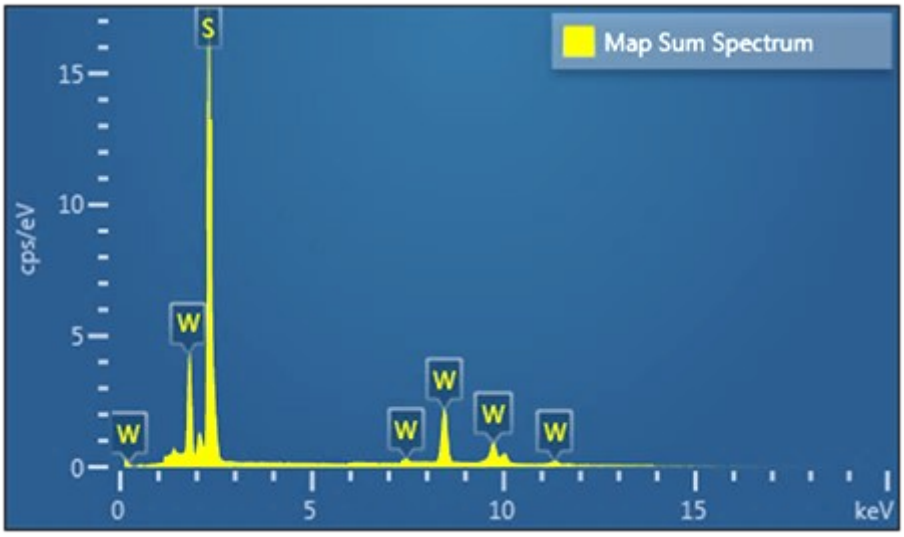

Figure S2. EDS profile of WS_2.

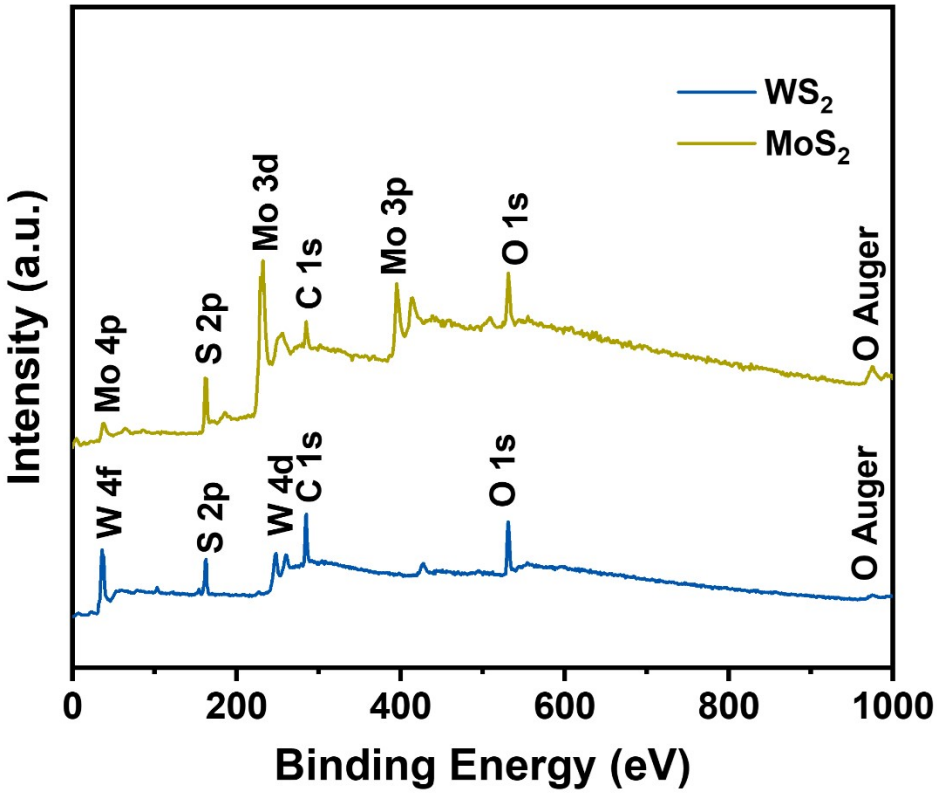

Figure S3. XPS survey profiles MoS_2 and WS_2.

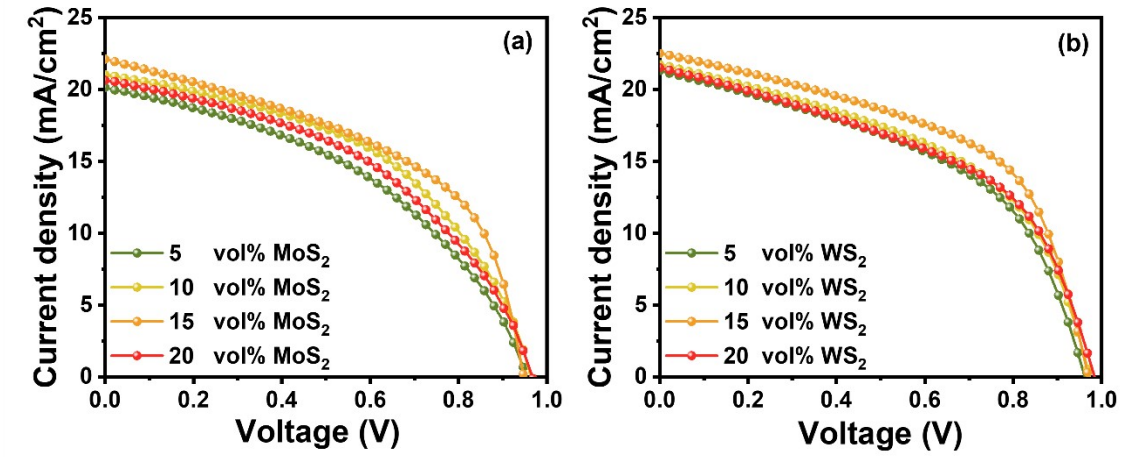

Figure S4. *J–V* characteristics of different amounts of (a) MoS_2 and (b) WS_2 using modulated $Cs_{0.1}MA_{0.9}PbI_3$ active layer in PSCs.

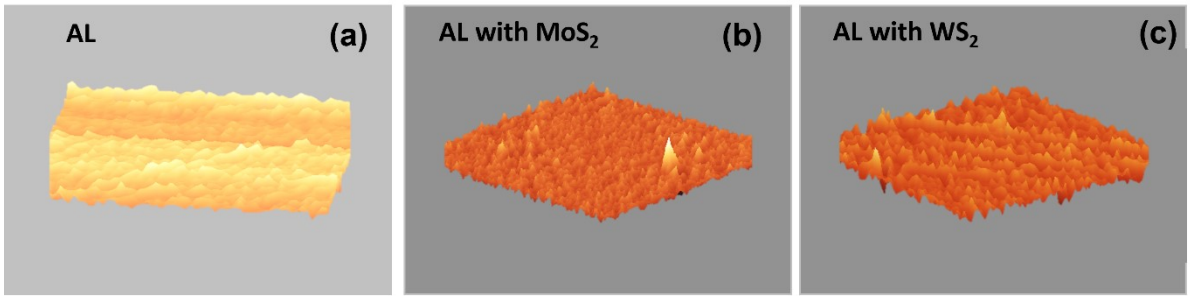

Figure S5. AFM images of (a) pure and (b) MoS_2, (c) WS_2-blended (15 vol.%) $Cs_{0.1}MA_{0.9}PbI_3$ perovskite layer.

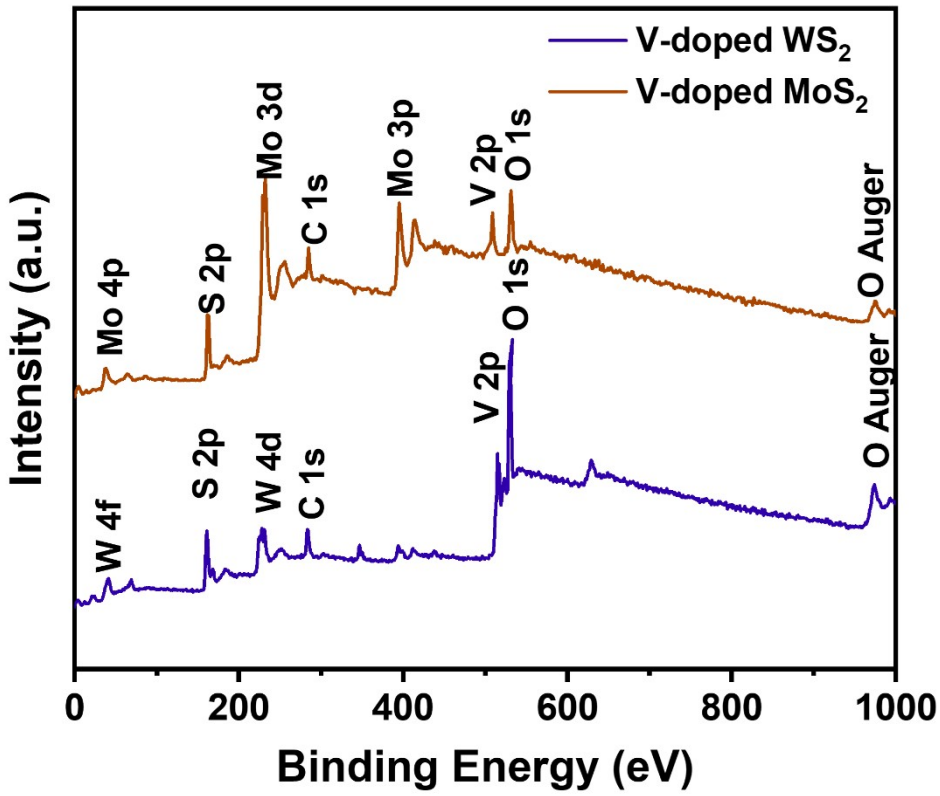

Figure S6. XPS survey profiles M2 and W2.

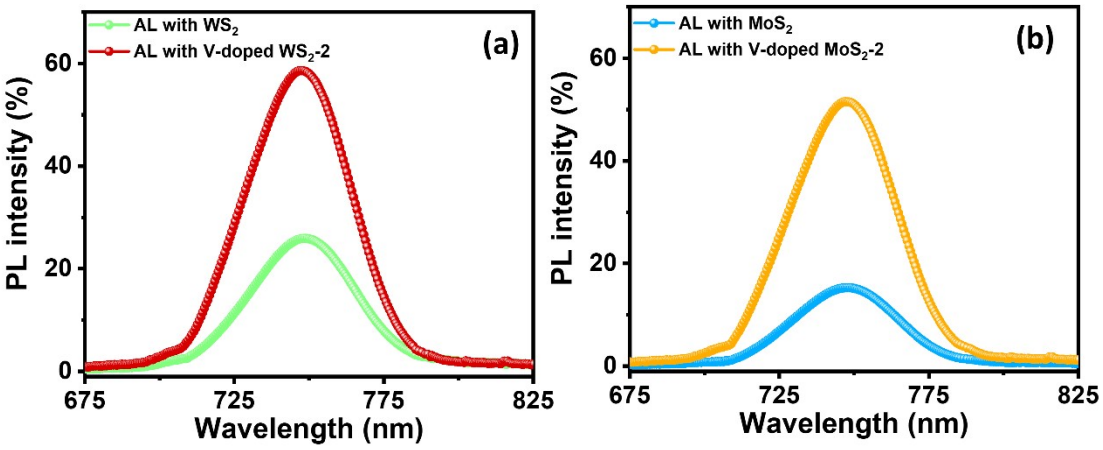

Figure S7. PL variations for the 15 vol% of (a) pure and W2 V-doped WS_2 suspended active layer; (b) pure and M2 V-doped MoS_2 suspended perovskite layer.

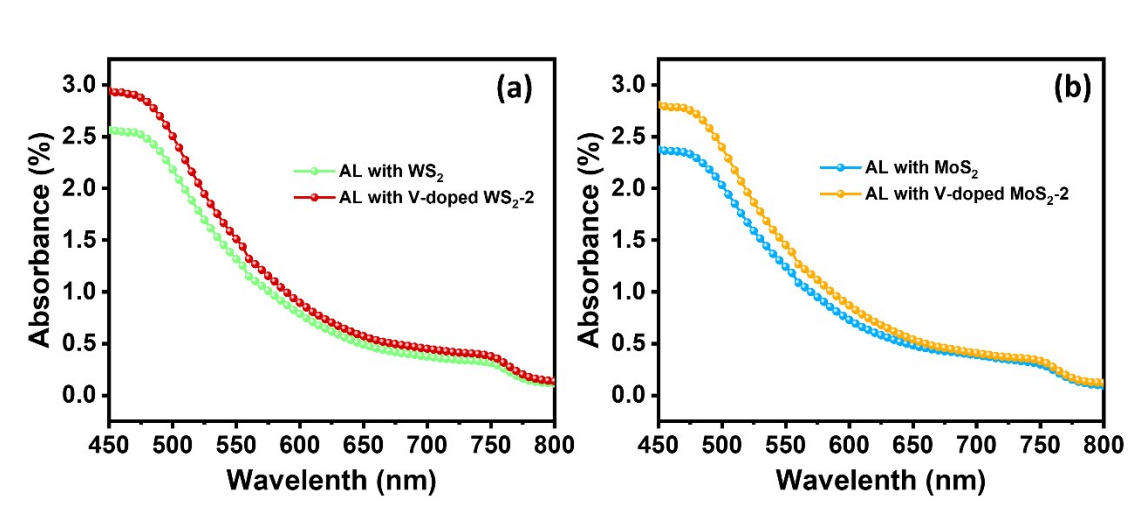

Figure S8. Absorption profile variations for the 15 vol% of (a) pure and W2 V-doped WS_2 suspended active layer; (b) pure and M2 V-doped MoS_2 suspended perovskite layer.

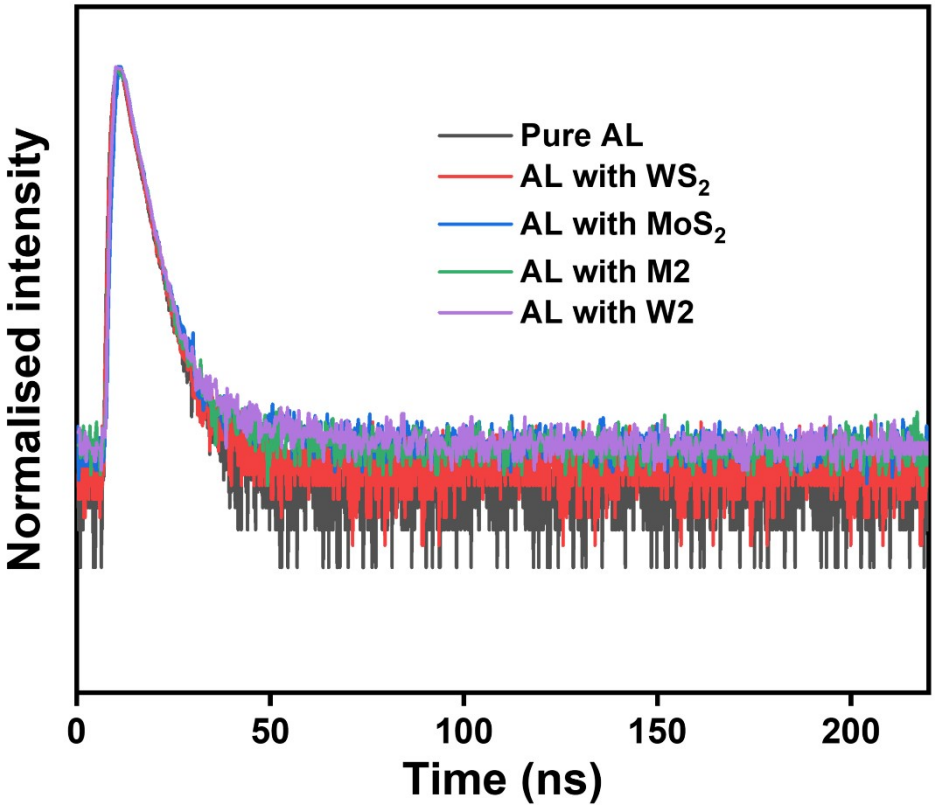

Figure S9. TRPL variations for the pure and 15 vol% of MoS_2, WS_2, M2 and W2 suspended perovskite layer.

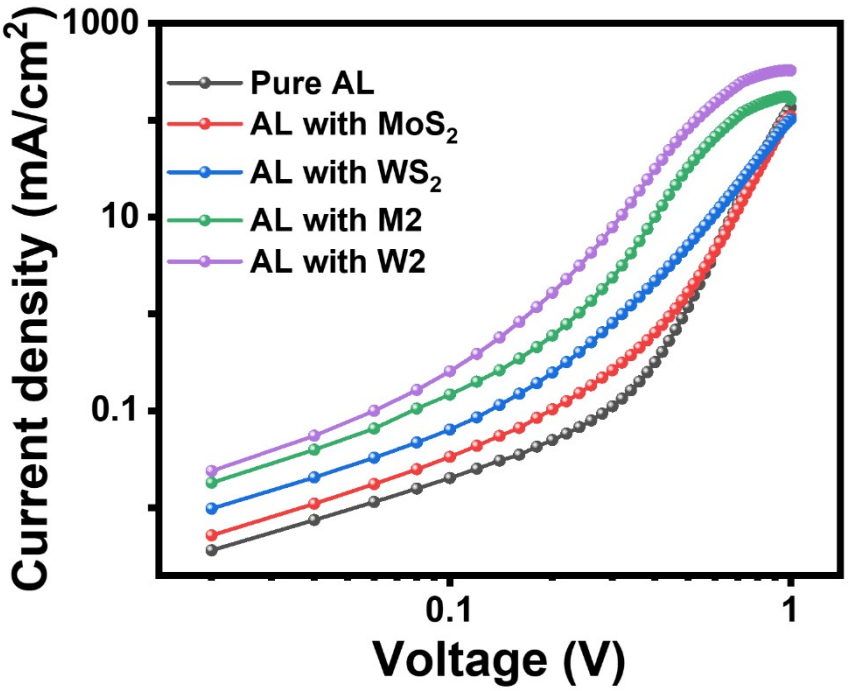

Figure S10. Log J-V variations for the pure and 15 vol% of MoS_2, WS_2, M2 and W2 suspended perovskite layer.

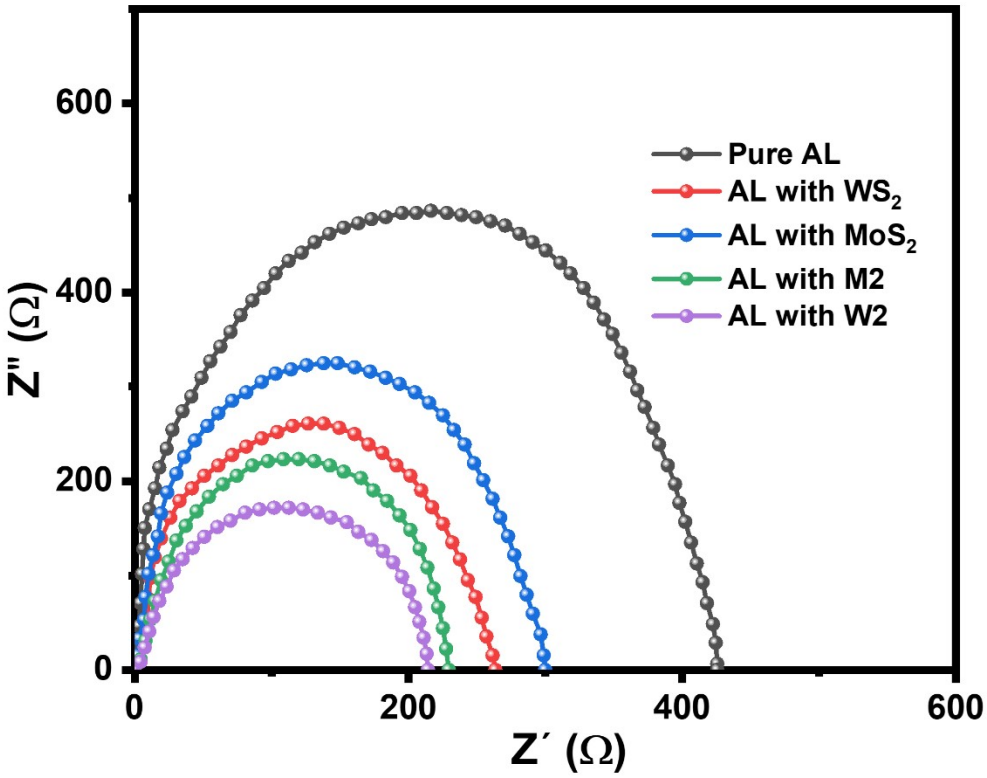

Figure S11. EIS profiles for the pure and 15 vol% of MoS_2, WS_2, M2 and W2 suspended perovskite layer.

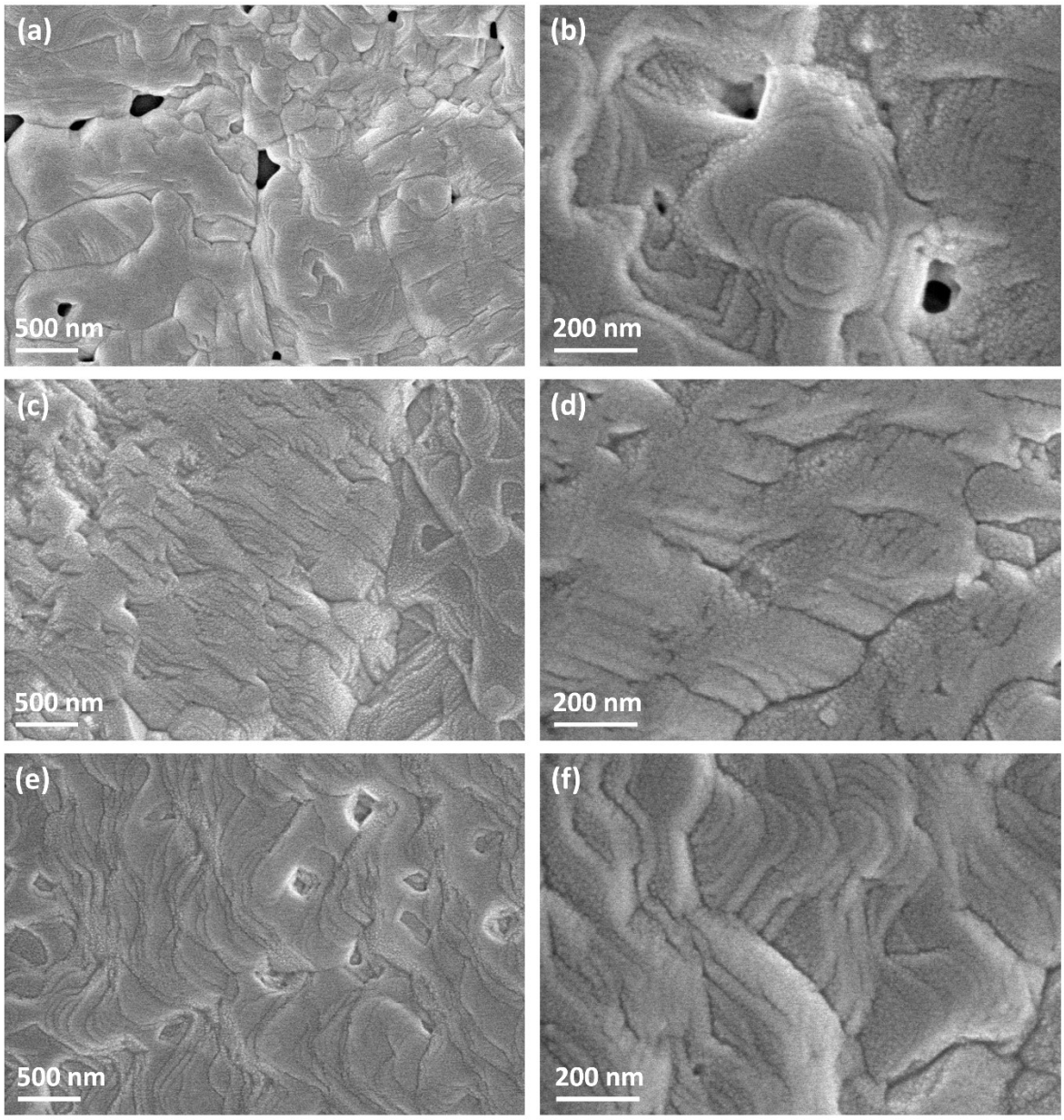

Figure S12. SEM images of (a-b) pure, (c-d) M2 V-doped MoS_2 and (e-f) W2 V-doped WS_2 suspended perovskite layer.

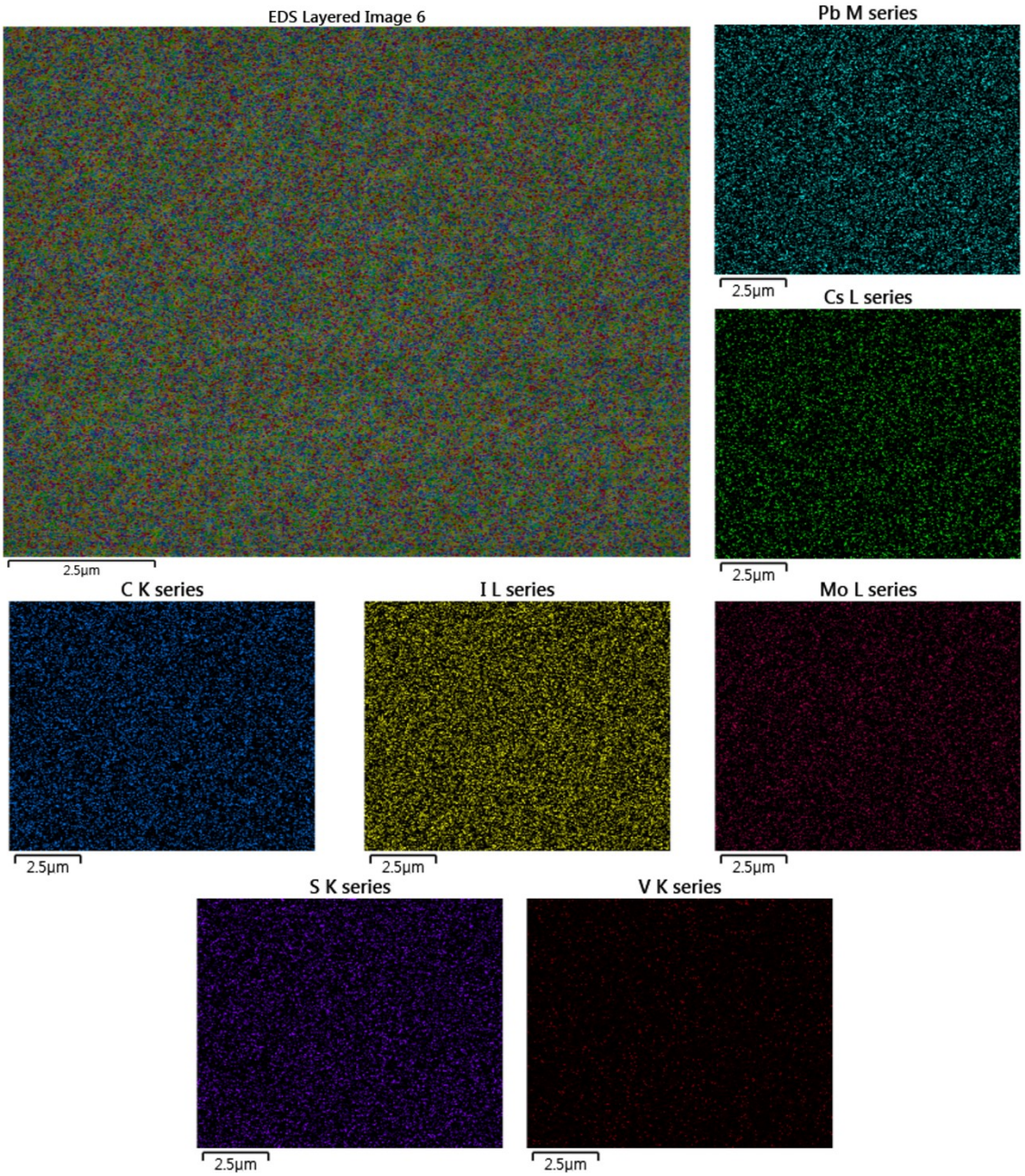

Figure S13. Elemental mapping images of M2 V-doped MoS_2 suspended perovskite layer.

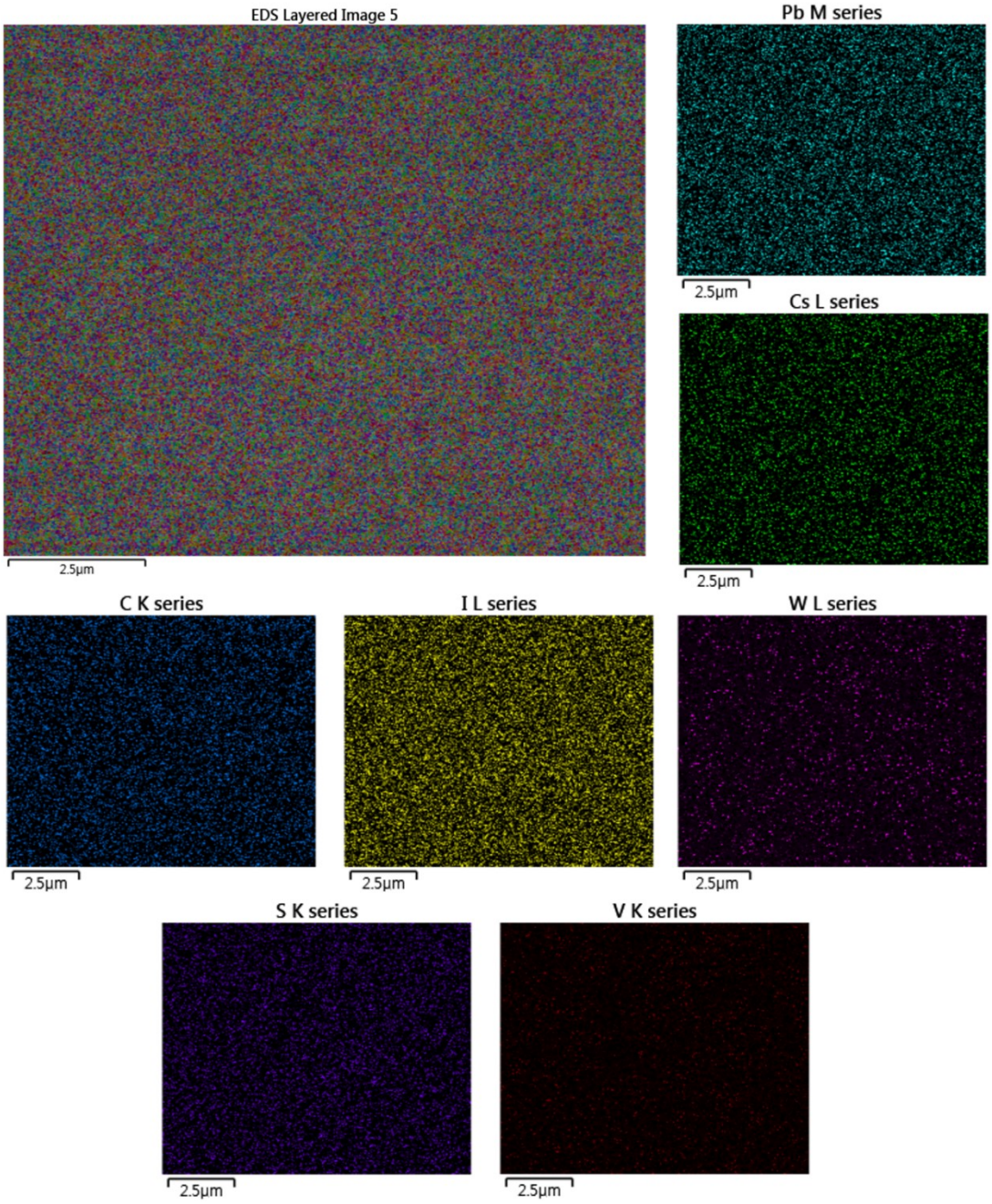

Figure S14. Elemental mapping images of W2 V-doped WS_2 suspended perovskite layer.

Table S1. Photovoltaic characteristics of PSC devices using different thickness of EL, HL and pure perovskite AL.

Active layer	**HTL thickness**	**ETL thickness**	**FF [%]**	**PCE [%]**
150 nm	40 nm	90 nm	48.1	7.53
205 nm	***40 nm***	***90 nm***	***55.4***	***10.55***
245 nm	40 nm	90 nm	51.3	8.85
205 nm	20 nm	90 nm	53.6	9.09
205 nm	55 nm	90 nm	54.2	9.99
205 nm	40 nm	75 nm	53.2	9.25
205 nm	55 nm	115 nm	52.5	9.51

Table S2. Photovoltaic characteristics of PSC devices using different concentration of MoS_2 and WS_2 nanostructures blended perovskite layer

Doping element	Amount of doping (vol.%)	V_{OC} [V]	J_{SC} [mA/cm^2]	FF [%]	PCE [%]	R_S [Ω·cm^2]
MoS_2	5	0.952	20.14	58.76	11.26	179.46
	10	0.964	21.0	58.13	11.77	176.24
	15	0.946	22.11	58.58	12.25	173.18
	20	0.967	20.64	57.70	11.51	178.43
WS_2	5	0.961	21.31	58.57	11.99	174.86
	10	0.968	21.73	57.81	12.16	169.32
	15	0.968	22.51	57.44	12.51	166.34
	20	0.984	21.51	57.15	12.09	171.76

Table S3. Photovoltaic characteristics of PSC devices using pure and different amount of V-doped XS_2 nanostructures blended perovskite layer

Active layer	**V_{OC} [V]**	**J_{SC} [mA/cm^2]**	**FF [%]**	**PCE [%]**	**R_S [Ω·cm^2]**
Pure Perovskite	0.945	20.1	55.4	10.54	181.78
Perovskite with M1	0.948	24.37	59.33	13.70	167.18
Perovskite with M2	0.975	24.76	61.57	14.86	154.63
Perovskite with M3	0.981	24.54	60.68	14.60	156.31
Perovskite with W1	0.971	23.33	59.58	13.49	163.75
Perovskite with W2	0.978	25.48	62.68	15.62	149.87
Perovskite with W2	0.989	24.65	61.10	14.89	151.47

Table S4. Photovoltaic characteristics of PSC devices using different concentrations of M2 and W2 nanostructures blended perovskite layer

Doping element	Amount of doping (vol.%)	V_{OC} [V]	J_{SC} [mA/cm^2]	FF [%]	PCE [%]	R_S [Ω·cm^2]
M2	5	0.968	22.56	60.15	13.13	165.34
	10	0.977	23.15	60.23	13.62	157.62
	15	0.975	24.76	61.57	14.86	154.63
	20	0.980	23.73	59.92	13.93	161.65
W2	5	0.961	23.85	62.14	14.21	156.34
	10	0.979	24.90	62.16	15.13	151.33
	15	0.978	25.49	62.68	15.62	149.87
	20	0.974	24.61	62.01	14.86	152.18

Table S5. Various perovskite-based solar cell **d**evice performances

Device structure	**Jsc ($mA \cdot cm^{-2}$)**	**V_{oc} (V)**	**FF (%)**	**PCE (%)**	**Ref.**
M2@$Cs_{0.1}MA_{0.9}PbI_3$	**24.76**	**0.975**	**61.57**	**14.86**	**This work**
W2@$Cs_{0.1}MA_{0.9}PbI_3$	**25.49**	**0.978**	**62.68**	**15.62**	
$CH_3NH_3PbI_3$	17.97	1.04	65.54	12.24	1
$MAPbI_{3-x}Cl_x/WS_2$ $MAPbI_{3-x}Cl_x/MoS_2$	15.91 14.89	0.82 0.96	64 0.67	8.02 9.53	2
$CH_3NH_3PbI_{3-x}Cl_x$ /PEG	19.53	0.94	70.35	12.90	3
$CH_3NH_3PbI_3$	18.84	1.09	66.70	13.69	4
WSe_2 $FASnI_3/WSe_2$	21.82 22.71	0.63 0.63	72 73.2	9.67 10.47	5
$CH_3NH_3PbI_3$ $CH_3NH_3PbI_3$/Urea	19.75 22.97	0.88 0.94	70.1 61.1	12.18 13.19	6
$CH_3NH_3PbI_3$	20.67	1.00	75	15.54	7
$MAPbI_3$ $MAPbI_3/MoS_2$	20.91 22.28	0.96 1.02	75.20 77.91	15.27 17.63	8
$MAPbI_3$ $MAPbI_3/MoS_2$	18.75 20.9	0.96 0.98	66 69	13.79 16.09	9
$CH_3NH_3PbI_3$	21.53	1.08	70.47	16.45	10
$CH_3NH_3PbI_3$ $CH_3NH_3PbI_3$/GO	18.11 20.71	0.927 0.959	73.1 76.3	12.3 15.2	11
$MAPbI_3/SnS_2$	19.29	0.68	61	13.04	12
$CH_3NH_3PbI_3/MoTe_2$	21.387	0.886	60	11.36	13

References

1. E. M. Mkawi, S. M. H. Qaid, I. S. Roqan, Y. Al-Hadeethi, F. G. Almehmadi, H. A. Alamoudi, F. Alreshidi, S. A. Alsulaiman, H. I. Jaafari, Y. Alajlani, A. Umar, E. Bekyarova and A. S. Aldwayyan, *Opt. Mater.*, 2024, **157**, 116089.
2. Y. G. Kim, K. C. Kwon, Q. Van Le, K. Hong, H. W. Jang and S. Y. Kim, *J. Power Sources*, 2016, **319**, 1–8.
3. C.-Y. Chang, C.-Y. Chu, Y.-C. Huang, C.-W. Huang, S.-Y. Chang, C.-A. Chen, C.-Y. Chao and W.-F. Su, *ACS Appl. Mater. Interfaces*, 2015, **7**, 4955–4961.
4. X. Jin, L. Yang and X.-F. Wang, *Nano-Micro Lett.*, 2021, **13**, 1–13.
5. T. Wang, F. Zheng, G. Tang, J. Cao, P. You, J. Zhao and F. Yan, *Adv. Sci.*, 2021, **8**, 2004315.
6. D. Thakur, J.-R. Wu, A. Chandel, K.-J. Cheng, S.-E. Chiang, K.-B. Cai, S.-H. Chen, C.-C. Yang, Y.-L. Zhong and C.-T. Yuan, *J. Alloy. Compd.*, 2021, **858**, 157660.
7. Z. Guo, L. Gao, Z. Xu, S. Teo, C. Zhang, Y. Kamata, S. Hayase and T. Ma, *Small*, 2018, **14**, 1802738.
8. Z. Liu, K. Liu, F. Zhang, S. M. Jain, T. He, Y. Jiang, P. Liu, J. Yang, H. Liu and M. Yuan, *Solar Energy*, 2020, **195**, 436–445.
9. K. Mahmood, A. Khalid, S. W. Ahmad, H. G. Qutab, M. Hameed and R. Sharif, *Solar Energy*, 2020, **203**, 32–36.
10. Y. Zhao, X. Zhang, X. Han, C. Hou, H. Wang, J. Qi, Y. Li and Q. Zhang, *Chem. Eng. J.*, 2021, **417**, 127912.
11. C.-C. Chung, S. Narra, E. Jokar, H.-P. Wu and E. W.-G. Diau, *J. Mater. Chem. A*, 2017, **5**, 13957–13965.
12. E. Zhao, L. Gao, S. Yang, L. Wang, J. Cao and T. Ma, *Nano Res.*, 2018, **11**, 5913–5923.
13. D. Vikraman, H. Liu, S. Hussain, S. H. A. Jaffery, K. Karuppasamy, E. B. Jo, Z. Abbas, J. Jung, J. Kang and H. S. Kim, *Small*, 2022, **18**, 2104216.